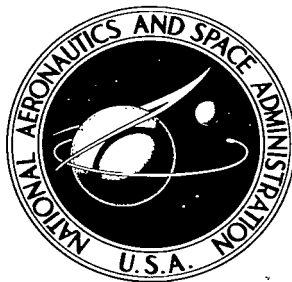


NASA TECHNICAL NOTE



NASA TN D-3634

c. 1

NASA TN D-3634



EFFECT OF WING LEADING-EDGE SHAPE  
ON AERODYNAMIC CHARACTERISTICS  
OF A 67° SWEEP WING-BODY MODEL  
AT MACH 1.50 TO 4.63

*by Robert G. Kyle and Maurice O. Feryn*

*Langley Research Center*

*Langley Station, Hampton, Va.*



EFFECT OF WING LEADING-EDGE SHAPE ON  
AERODYNAMIC CHARACTERISTICS OF A  
67° SWEPT WING-BODY MODEL AT  
MACH 1.50 TO 4.63

By Robert G. Kyle and Maurice O. Feryn

Langley Research Center  
Langley Station, Hampton, Va.

NATIONAL AERONAUTICS AND SPACE ADMINISTRATION

---

For sale by the Clearinghouse for Federal Scientific and Technical Information  
Springfield, Virginia 22151 - Price \$1.00

EFFECT OF WING LEADING-EDGE SHAPE ON  
AERODYNAMIC CHARACTERISTICS OF A  
67° SWEEP WING-BODY MODEL AT  
MACH 1.50 TO 4.63

By Robert G. Kyle and Maurice O. Feryn  
Langley Research Center

SUMMARY

An investigation has been made to determine the effects of wing leading-edge shape on the stability characteristics of a 67° swept wing-body model. Three leading-edge shapes were tested: a sharp wedge section, a slightly rounded section, and a relatively blunt section. Tests were performed at angles of attack from about  $-4^\circ$  to  $10^\circ$ , at angles of sideslip from about  $-4^\circ$  to  $6^\circ$ , and at a Reynolds number per foot of  $3.0 \times 10^6$  ( $9.84 \times 10^6$  per meter). The results of this investigation indicate that increasing leading-edge bluntness increases the effective dihedral for wings with subsonic leading edges and reduces the effective dihedral for wings with supersonic leading edges. Increasing leading-edge bluntness has little effect on the longitudinal aerodynamic characteristics, other than to increase the minimum drag coefficient and to reduce the lift-drag ratio.

INTRODUCTION

The stability and performance characteristics of supersonic cruise aircraft are, among other things, dependent upon the relationship between the wing sweep and the Mach number. In particular, when the wing leading edge is swept behind the Mach cone it is possible to take advantage of wing camber and twist to improve the performance characteristics through a reduction in drag due to lift. This relationship between wing sweep and the Mach number also influences the stability characteristics, however, with one of the effects being a generally higher level of effective dihedral for wings swept behind the Mach cone than for wings swept ahead of the Mach cone. (See refs. 1 to 3, for example.) In addition, another geometric parameter affecting the aerodynamic behavior of a wing is the shape of the wing leading-edge cross section. A rounded section should be more efficient for a subsonic wing and a sharp section more efficient for a supersonic wing. In order to demonstrate some of the effects of leading-edge shape on supersonic cruise flight, a wind-tunnel investigation of a wing-body model having a 67° swept wing was undertaken with three alternate leading-edge shapes varying from a sharp wedge to a blunt

rounded shape. The model with each of the leading-edge shapes was tested over a range of Mach numbers from 1.50 to 4.63 so that conditions of both subsonic and supersonic leading edges were obtained.

The investigation was performed in the Langley Unitary Plan wind tunnel at angles of attack from about  $-4^{\circ}$  to  $10^{\circ}$  and angles of sideslip from about  $-4^{\circ}$  to  $6^{\circ}$ . Most of the tests were performed at a Reynolds number per foot of  $3.0 \times 10^6$  ( $9.84 \times 10^6$  per meter).

## SYMBOLS

The lateral force and moment data are referenced to the body-axis system, and the longitudinal force and moment data are referenced to the stability-axis system. The reference moment center was located 24.105 inches (61.227 cm) behind the nose of the fuselage on the body center line.

The symbols are defined as follows:

b	wing span, 1.667 feet (0.5080 meter)
$\bar{c}$	mean aerodynamic chord, 0.9896 foot (0.3016 meter)
$C_D$	drag coefficient, Drag/qS
$C_L$	lift coefficient, Lift/qS
$C_m$	pitching-moment coefficient, Pitching moment/qS $\bar{c}$
$C_l$	rolling-moment coefficient, Rolling moment/qSb
$C_{l\beta}$	effective-dihedral parameter, $\frac{\Delta C_l}{\Delta \beta}$ , per degree
$C_{l\beta\alpha} = \frac{\Delta C_l / \Delta \beta}{\Delta \alpha}$	
$C_n$	yawing-moment coefficient, Yawing moment/qSb
$C_{n\beta}$	directional-stability parameter, $\frac{\Delta C_n}{\Delta \beta}$ , per degree
$C_Y$	side-force coefficient, Side force/qS

$C_{Y\beta}$	side-force parameter, $\frac{\Delta C_Y}{\Delta \beta}$ , per degree
L/D	lift-drag ratio
M	Mach number
q	free-stream dynamic pressure, pounds/foot <sup>2</sup> (newtons/meter <sup>2</sup> )
S	reference wing area, 1.389 feet <sup>2</sup> (0.12905 meter <sup>2</sup> )
x,y	airfoil section coordinates, inches (centimeters)
$\alpha$	angle of attack, degrees
$\beta$	angle of sideslip, degrees

## APPARATUS AND TESTS

### Model

Geometric details and a photograph of the model are presented in figure 1. Airfoil coordinates are presented in table I. The configuration had a mid-wing with zero dihedral and a cylindrical fuselage with an ogive nose. The wing was composed of a slab-shaped main spar to which various leading-edge extensions could be attached. Three leading-edge extensions were tested: one having a sharp wedge section ( $W_S$ ), and the other two having rounded sections ( $W_B$  and  $W_{6B}$ ), extension  $W_{6B}$  having a leading-edge radius six times that of  $W_B$ . For each leading-edge configuration, the wing had a sweep of  $67^\circ$ , an aspect ratio of 2.00, and thicknesses that varied from 2.65 percent chord at the wing-body juncture to 6.0 percent chord at the tip.

### Tunnel

Tests were conducted in both the low and high Mach number test sections of the Langley Unitary Plan wind tunnel, which is a variable-pressure continuous-flow tunnel. Each test section is approximately 4 feet square and 7 feet long. The nozzles leading to the test sections are the asymmetric sliding-block type that permit a continuous variation in Mach number from about 1.5 to 2.9 in the low Mach number test section and from about 2.3 to 4.7 in the high Mach number test section.

## Test Conditions

The stagnation temperatures and pressures for the various test Mach numbers are as follows:

Mach number	Stagnation temperature, °F (°K)	Stagnation pressure, psia (N/cm <sup>2</sup> )
1.50	150 (338.7)	11.58 ( 7.98)
1.90	150 (338.7)	13.22 ( 9.11)
2.30	175 (352.6)	15.92 (10.98)
2.60	175 (352.6)	18.65 (12.86)
2.96	175 (352.6)	22.57 (15.56)
3.95	175 (352.6)	39.94 (27.54)
4.63	175 (352.6)	54.74 (37.74)

For the results that are presented herein, the Reynolds number per foot was constant at  $3.0 \times 10^6$  ( $9.84 \times 10^6$  per meter). The stagnation dewpoint was maintained at  $-30^\circ \text{F}$  ( $238.6^\circ \text{K}$ ) in order to avoid condensation effects.

The model had boundary-layer transition strips,  $1/16$  inch (0.1588 cm) wide, composed of No. 60 carborundum grains set in a plastic adhesive located 1.2 inches (3.048 cm) behind the body apex and 0.4 inch (1.016 cm) in a streamwise direction behind the wing leading edge. Limited tests were made over a Reynolds number range for the model with free transition and with No. 80 carborundum grains in order to confirm that the test conditions provided a turbulent boundary layer. These additional tests indicated no effect of Reynolds number or transition strips on the incremental effects of leading-edge-shape changes.

The configurations were tested through an angle-of-attack range from about  $-4^\circ$  to  $10^\circ$  and through an angle-of-sideslip range of  $-4^\circ$  to  $6^\circ$ .

## Measurements

Aerodynamic forces and moments were measured by means of a six-component electrical strain-gage balance housed within the model. The balance was rigidly fastened to a sting support which was in turn attached to the tunnel support system. The balance-chamber pressure was measured by means of a single static-pressure orifice located in the balance cavity.

## Accuracy

The accuracy of the individual measured quantities, based on calibrations and repeatability of data, is estimated to be within the following limits:

$C_D$ . . . . .	$\pm 0.0003$
$C_L$ . . . . .	$\pm 0.002$
$C_l$ . . . . .	$\pm 0.0005$
$C_m$ . . . . .	$\pm 0.002$
$C_n$ . . . . .	$\pm 0.002$
$C_Y$ . . . . .	$\pm 0.001$
$\alpha$ , deg . . . . .	$\pm 0.10$
$\beta$ , deg . . . . .	$\pm 0.10$
$M = 1.50$ to $2.96$ . . . . .	$\pm 0.015$
$M = 3.95$ and $4.63$ . . . . .	$\pm 0.050$

## Corrections

Angles of attack were corrected to tunnel-flow angularity, and angles of attack and sideslip were corrected for deflection of the balance and sting support due to aerodynamic loads. The drag data were adjusted to correspond to free-stream static conditions at the base of the model.

## DISCUSSION

### Longitudinal Aerodynamic Characteristics

The effects of leading-edge shape on the aerodynamic characteristics in pitch of the wing-body vehicle are presented in figure 2. These data indicate only a small effect of leading-edge shape on lift-curve slope and pitching moment, although at all test Mach numbers, increasing leading-edge bluntness produces noticeable increases in drag coefficient and decreases in lift-drag ratio. The increase in minimum drag due to the blunter leading edge appears to be somewhat more noticeable at the higher Mach numbers, as might be expected when the leading edge of the wing is supersonic.

### Lateral Aerodynamic Characteristics

Typical aerodynamic characteristics in sideslip are presented in figures 3 and 4. These figures are presented to show the linearity of the data since all lateral parameters presented herein were obtained from incremental results of tests made throughout the angle-of-attack range at sideslip angles of about  $0^\circ$  and  $2^\circ$ . These data show that the variations of the lateral coefficients with sideslip angle are essentially linear at all test Mach numbers throughout the angle-of-sideslip range of these tests.

The effects of leading-edge shape on the variation of the lateral parameters with angle of attack are presented in figures 5 to 7. Little or no effect of leading-edge shape on  $C_{Y\beta}$  or  $C_{n\beta}$  exists at any of the test Mach numbers. However, there is an effect on the variation of  $C_{l\beta}$  with  $\alpha$  that varies with Mach number, and this effect is summarized in figure 8 in terms of the slope  $C_{l\beta\alpha}$  (measured near  $\alpha = 0^\circ$ ) as a function of Mach number.

The results presented in figure 8 show that all configurations have relatively large negative values of  $C_{l\beta\alpha}$  at the lower Mach numbers, and that these values decrease rapidly up to a Mach number of about 2.6. These results are characteristic of swept-wing configurations which generally provide large negative values of  $C_{l\beta\alpha}$  when the wing leading edge is subsonic with these values decreasing toward zero as the wing leading edge approaches the supersonic condition. (For the leading-edge sweep angle of  $67^\circ$ , the sonic leading edge occurs at about  $M = 2.56$ .) For Mach numbers above about 2.6, the results of figure 8 indicate a slight increase in the negative values of  $C_{l\beta\alpha}$ . This increase is believed to be due to the finite wing tips acting as subsonic wing leading edges. (This phenomenon is discussed in ref. 1.)

The data of figure 8 also show that at the lower test Mach numbers, for which the wing leading edge is subsonic, increased leading-edge bluntness leads to increased values of positive effective dihedral  $-C_{l\beta}$ . On the other hand, at the higher test Mach numbers for which the wing leading edge is supersonic, increased leading-edge bluntness leads to decreased values of positive effective dihedral. This effect is probably related to the slightly higher panel lift-curve slope that might be expected for the wings with blunter leading edges at the Mach numbers corresponding to a subsonic leading edge, whereas at the Mach numbers corresponding to a supersonic leading edge, the better lift capability might be expected for the wing with the sharp leading edge. It thus appears that a moderate variation in effective dihedral may result from varying the wing leading-edge bluntness of aircraft configurations; however, at supersonic-flight Mach numbers, the direction of this variation is dependent on the relationship between wing sweep and the Mach number.

## CONCLUSIONS

An investigation made to determine the effects of the shape of the wing leading-edge cross section on the stability characteristics of a  $67^\circ$  swept wing-body model at Mach numbers from 1.50 to 4.63 indicated the following conclusions:

1. Increasing leading-edge bluntness has little effect on the longitudinal aerodynamic characteristics, other than to increase the minimum drag coefficient and reduce the lift-drag ratio.



2. Increasing leading-edge bluntness produces increased effective dihedral for wings with subsonic leading edges and reduced effective dihedral for wings with supersonic leading edges.

Langley Research Center,

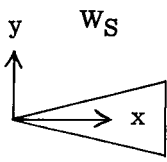
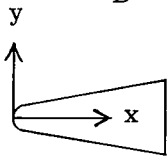
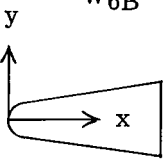
National Aeronautics and Space Administration,

Langley Station, Hampton, Va., June 1, 1966.

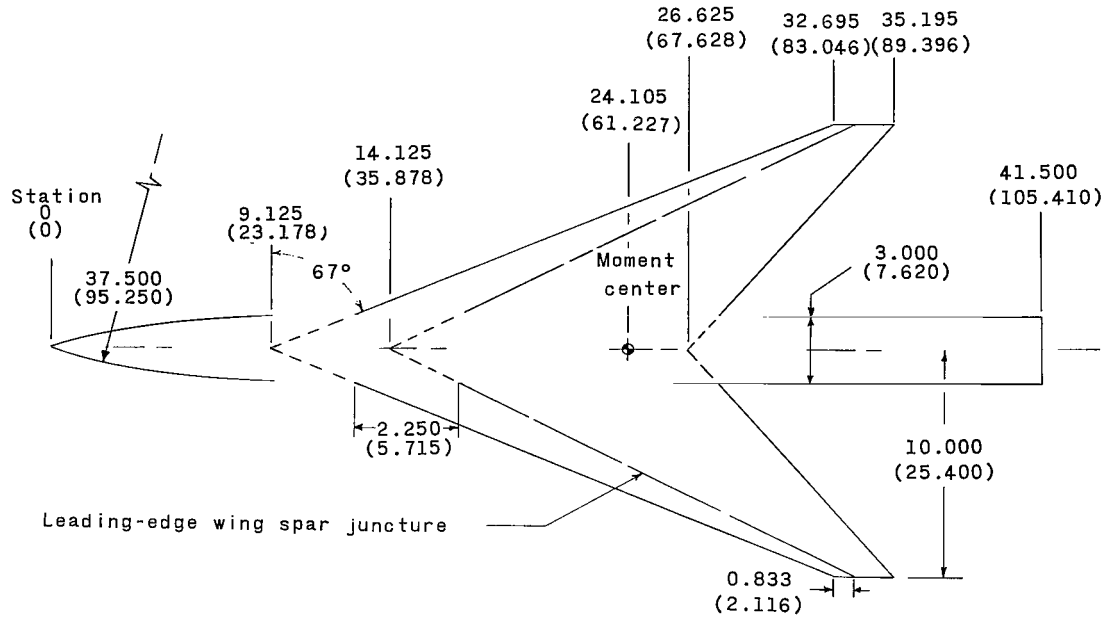
#### REFERENCES

1. Sherman, Windsor L.; and Margolis, Kenneth: Theoretical Calculations of the Effects of Finite Sideslip at Supersonic Speeds on the Span Loading and Rolling Moment for Families of Thin Sweptback Tapered Wings at an Angle of Attack. NACA TN 3046, 1953.
2. Feryn, Maurice O.; and Campbell, James F.: Effects of Wing Dihedral and Planform on Stability Characteristics of a Research Model at Mach Numbers From 1.80 to 4.63. NASA TN D-2914, 1965.
3. Fuller, Dennis E.; and Feryn, Maurice: Effect of Wing Height and Dihedral on Stability Characteristics of a  $76^\circ$  Swept Wing Body at Mach Numbers From 1.60 to 4.63. NASA TM X-1023, 1964.

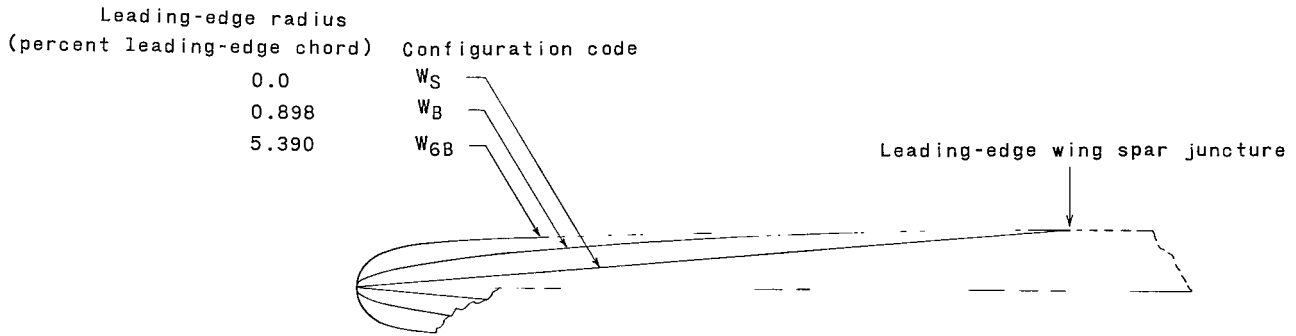
TABLE I.- AIRFOIL COORDINATES

Leading-edge section	Coordinates at wing-body juncture <sup>1</sup>				Coordinates at tip			
	x		y		x		y	
	in.	cm	in.	cm	in.	cm	in.	cm
 <p>WS</p>	0	0	0	0	0	0	0	0
	2.250	5.715	.202	.513	.833	2.116	.075	.190
	15.250	38.735	.202	.513	2.500	6.350	.075	.190
 <p>WB</p>	0	0	0	0	0	0	0	0
	.085	.216	.052	.132	.031	.079	.019	.048
	.169	.429	.071	.180	.063	.160	.026	.066
	.338	.859	.099	.251	.125	.318	.037	.094
	.675	1.715	.136	.345	.250	.635	.050	.127
	1.013	2.573	.161	.409	.375	.953	.060	.152
	1.350	3.429	.179	.455	.500	1.270	.067	.170
	1.688	4.288	.192	.488	.625	1.587	.071	.180
	2.025	5.144	.200	.508	.750	1.905	.074	.188
	2.250	5.715	.202	.513	.833	2.116	.075	.190
	15.250	38.735	.202	.513	2.500	6.350	.075	.190
 <p>W6B</p>	0	0	0	0	0	0	0	0
	.003	.008	.025	.063	.002	.005	.010	.025
	.011	.028	.050	.127	.009	.023	.020	.051
	.028	.071	.075	.191	.018	.046	.030	.076
	.052	.132	.100	.254	.035	.089	.040	.102
	.088	.223	.125	.317	.057	.145	.050	.127
	.147	.373	.150	.381	.072	.183	.055	.140
	.255	.648	.175	.445	.101	.257	.060	.152
	.405	1.029	.185	.470	.118	.300	.062	.157
	.650	1.651	.195	.495	.153	.389	.065	.165
	.813	2.065	.200	.508	.184	.467	.067	.170
	2.250	5.715	.202	.513	.233	.592	.070	.179
	15.250	38.735	.202	.513	.278	.706	.074	.188
					.833	2.116	.075	.190
					2.500	6.350	.075	.190

<sup>1</sup>At wing-body juncture, x is measured from body station 12.660 inches (32.156 cm).

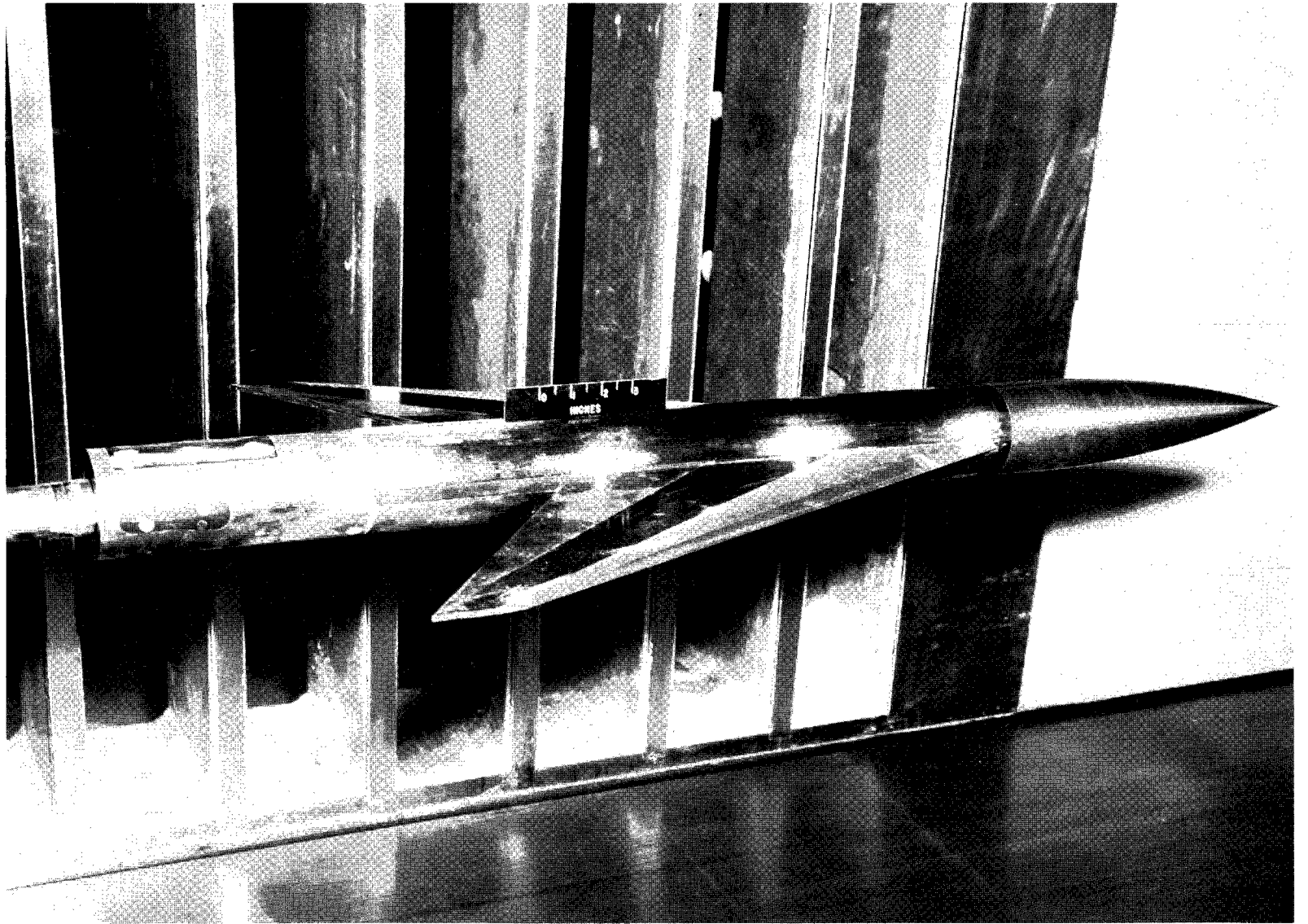


Typical leading-edge section



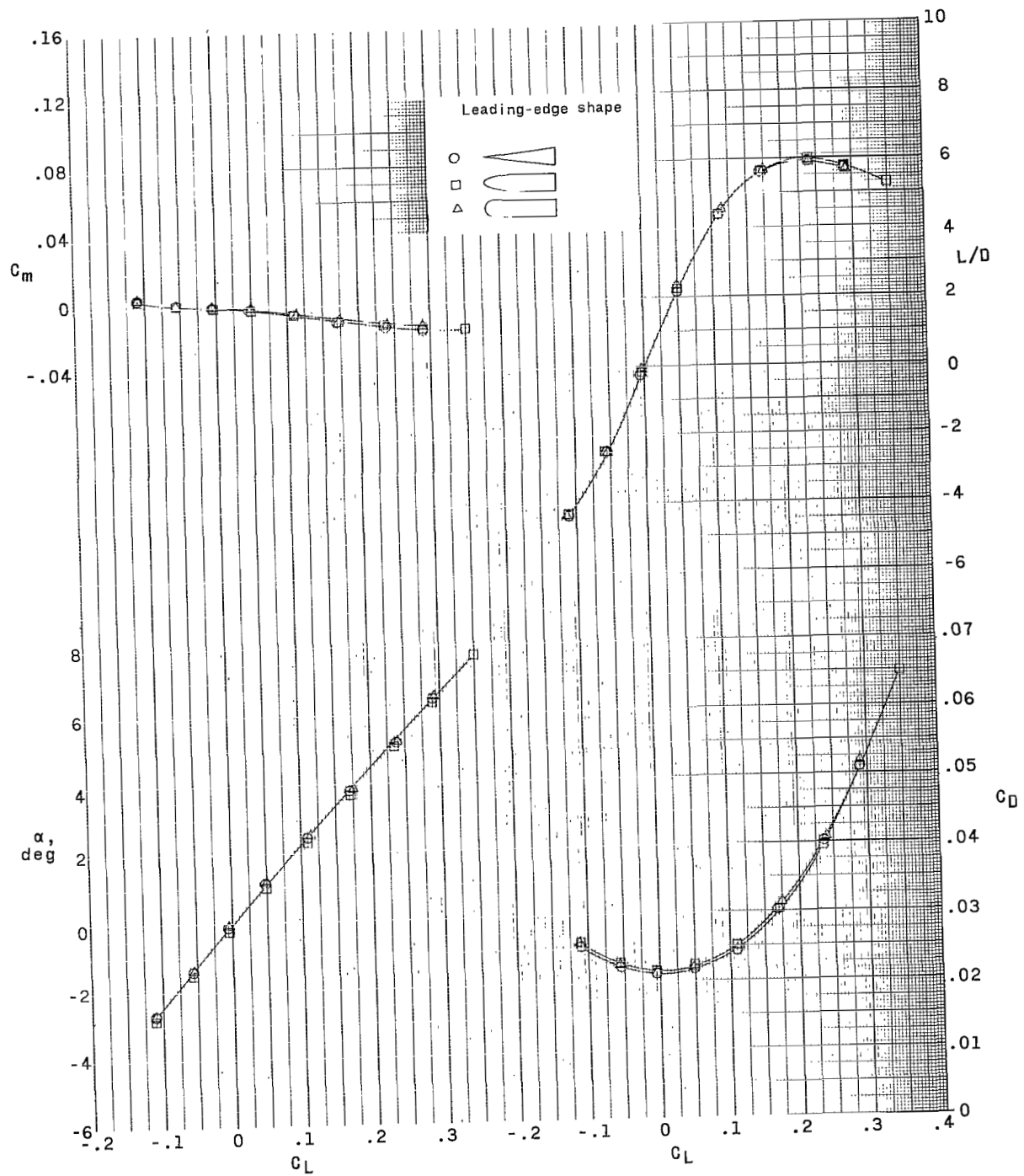
(a) Model details. Dimensions are given in inches and parenthetically in centimeters unless otherwise noted.

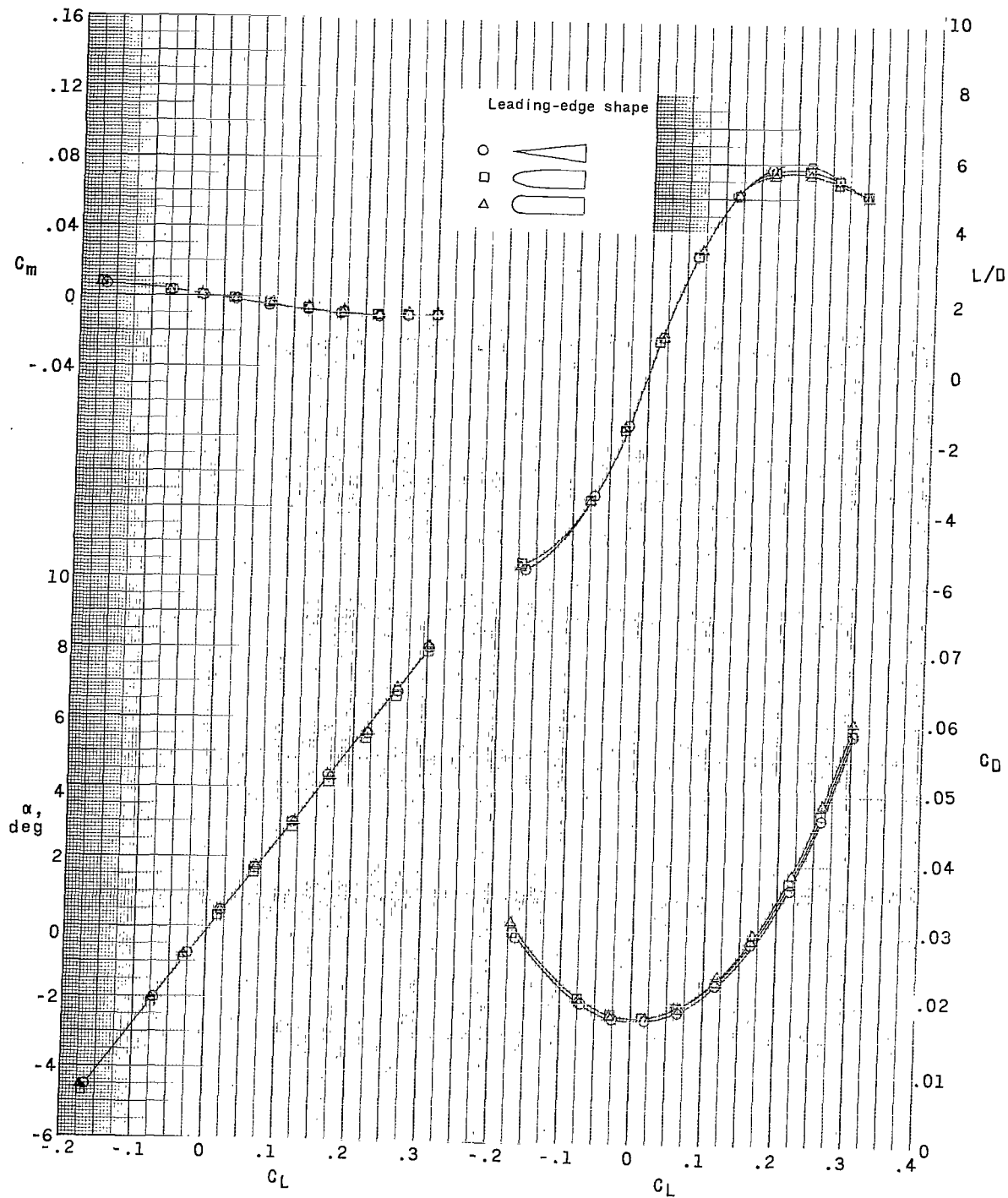
Figure 1.- Model.



(b) Photograph of model with leading-edge configuration  $W_S$ . L-65-5209

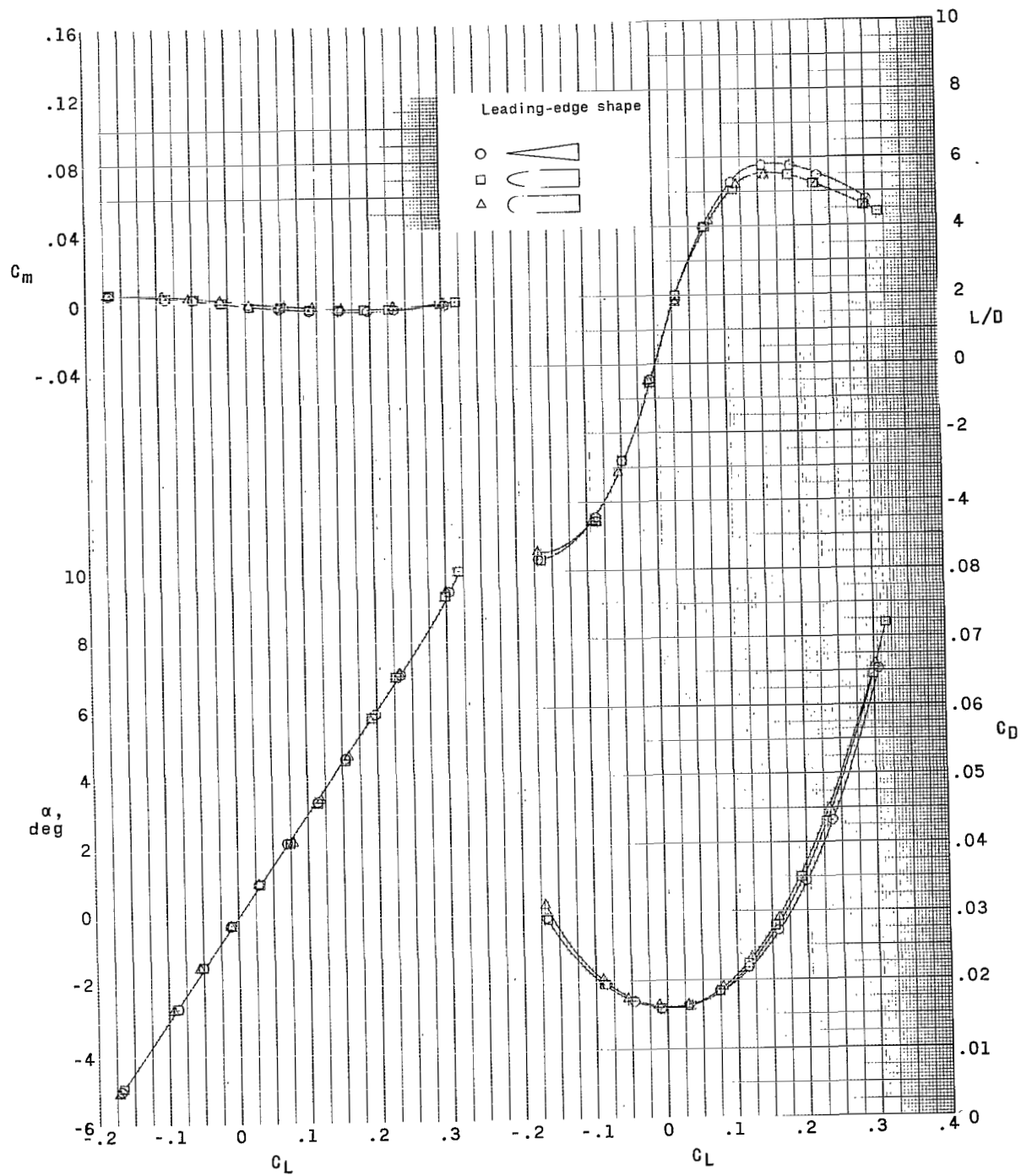
Figure 1.- Concluded.





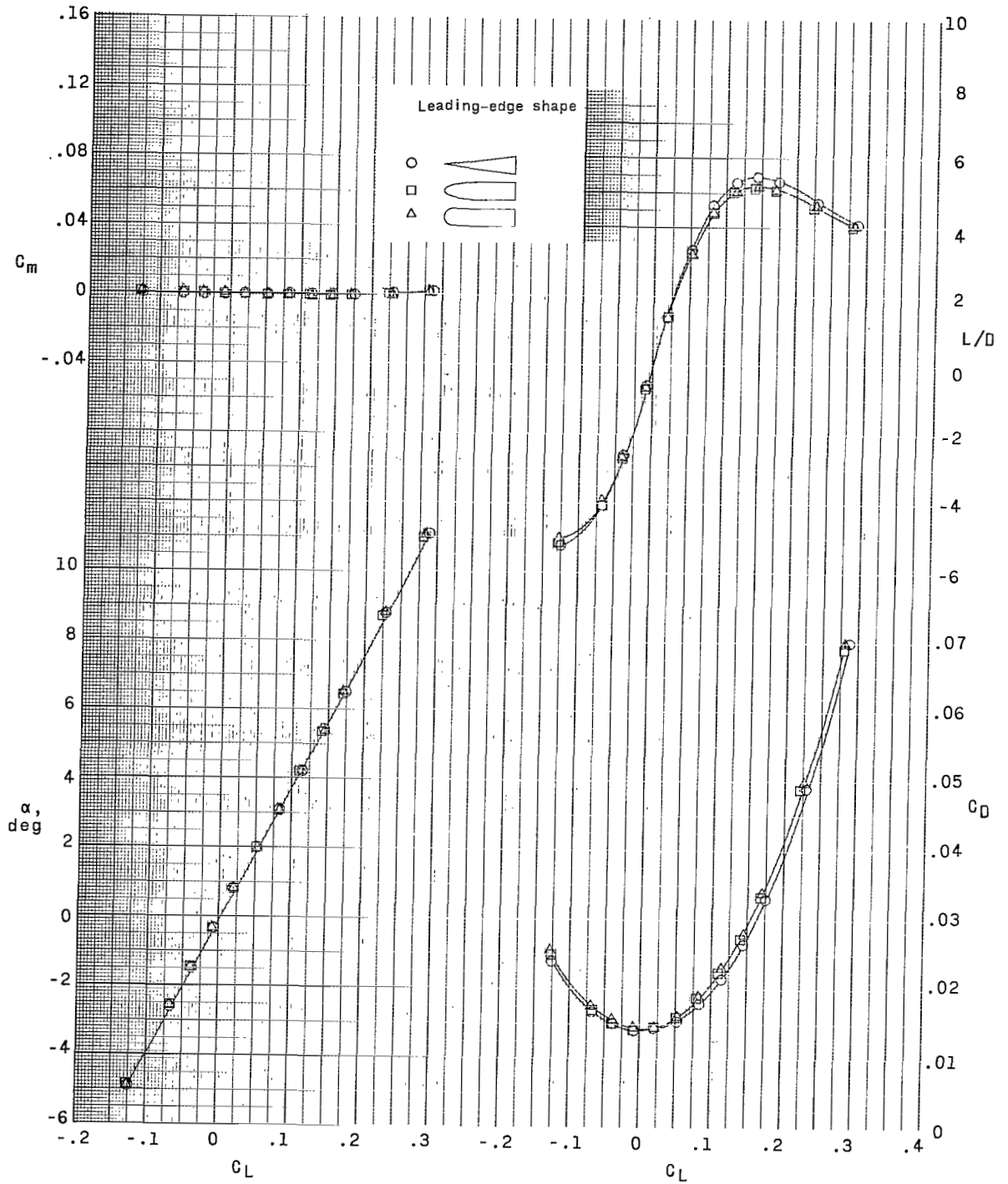
(b)  $M = 1.90$ .

Figure 2.- Continued.



(c) M = 2.30.

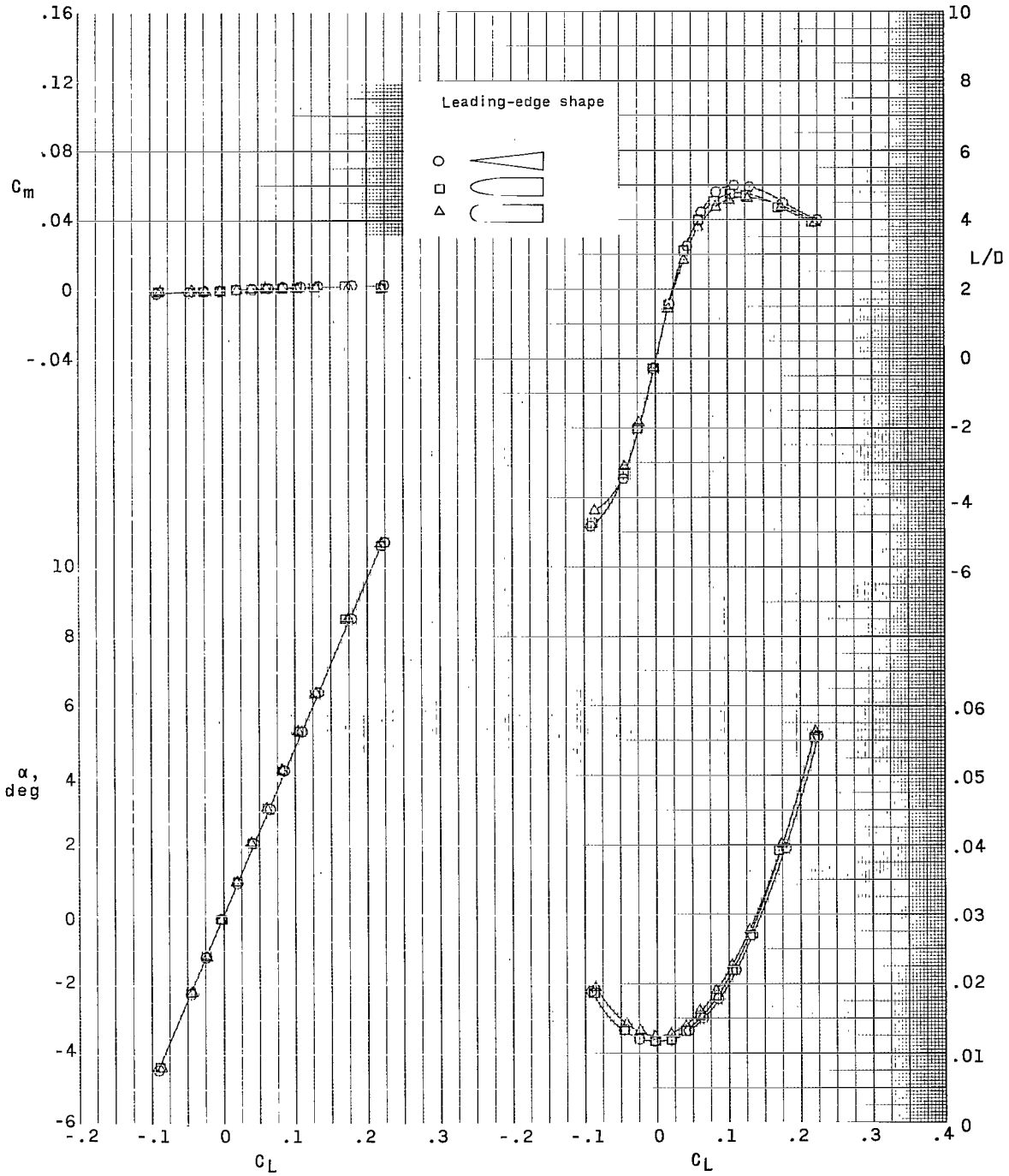
Figure 2.- Continued.



(d)  $M = 2.96$ .

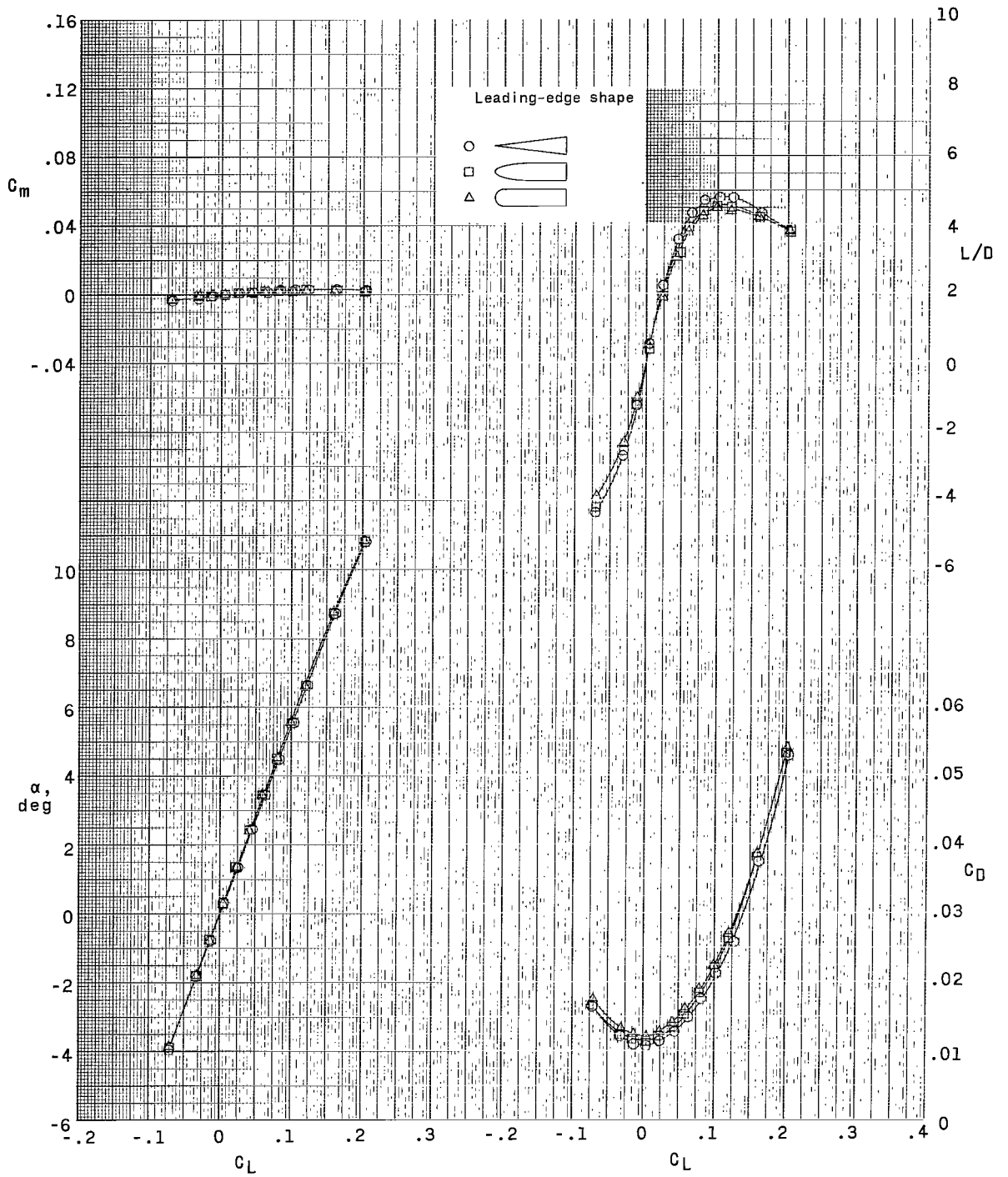
Figure 2.- Continued.





(e)  $M = 3.95$ .

Figure 2.- Continued.



(f)  $M = 4.63$ .

Figure 2.- Concluded.

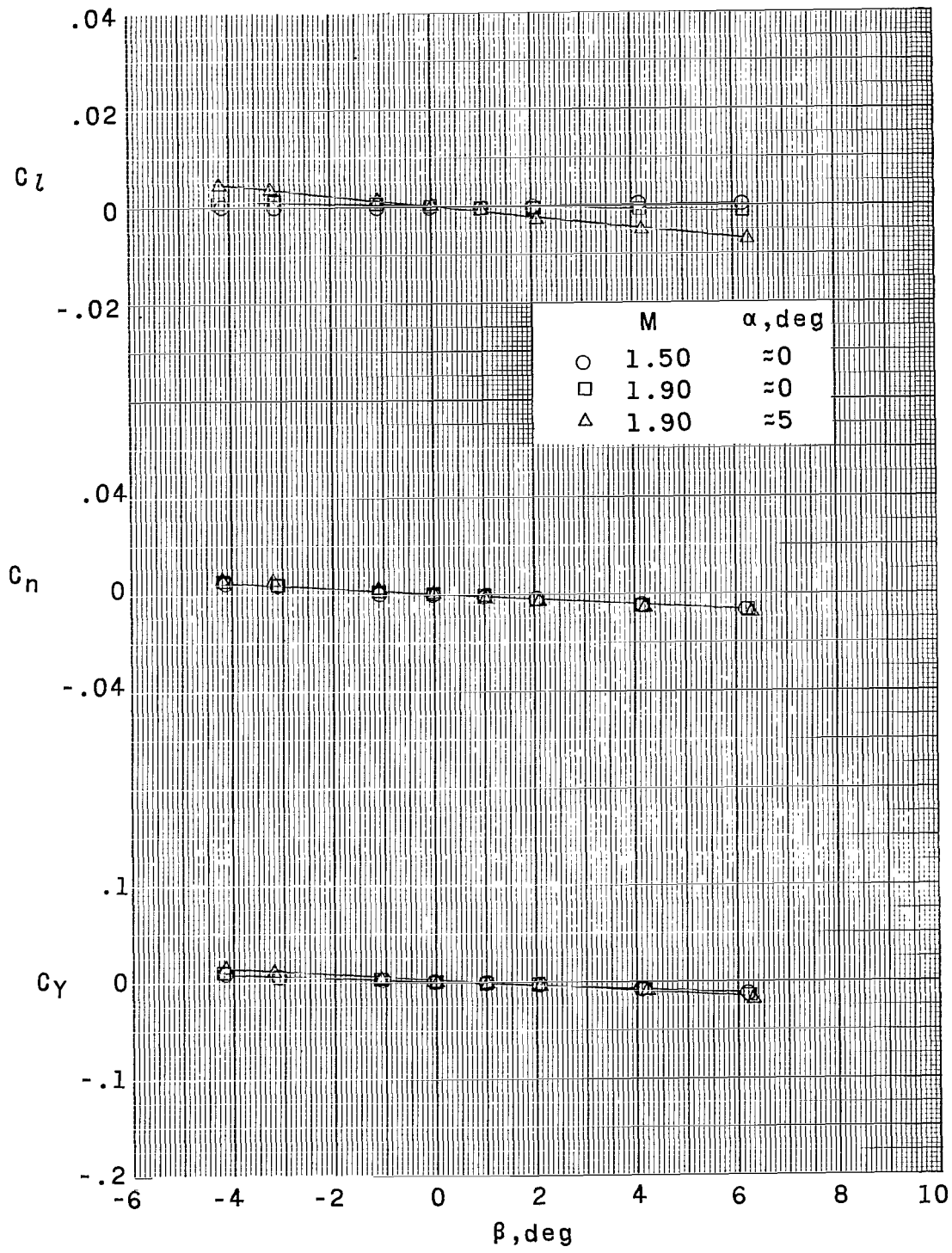


Figure 3.- Typical aerodynamic characteristics in sideslip for leading-edge configuration  $W_B$ .

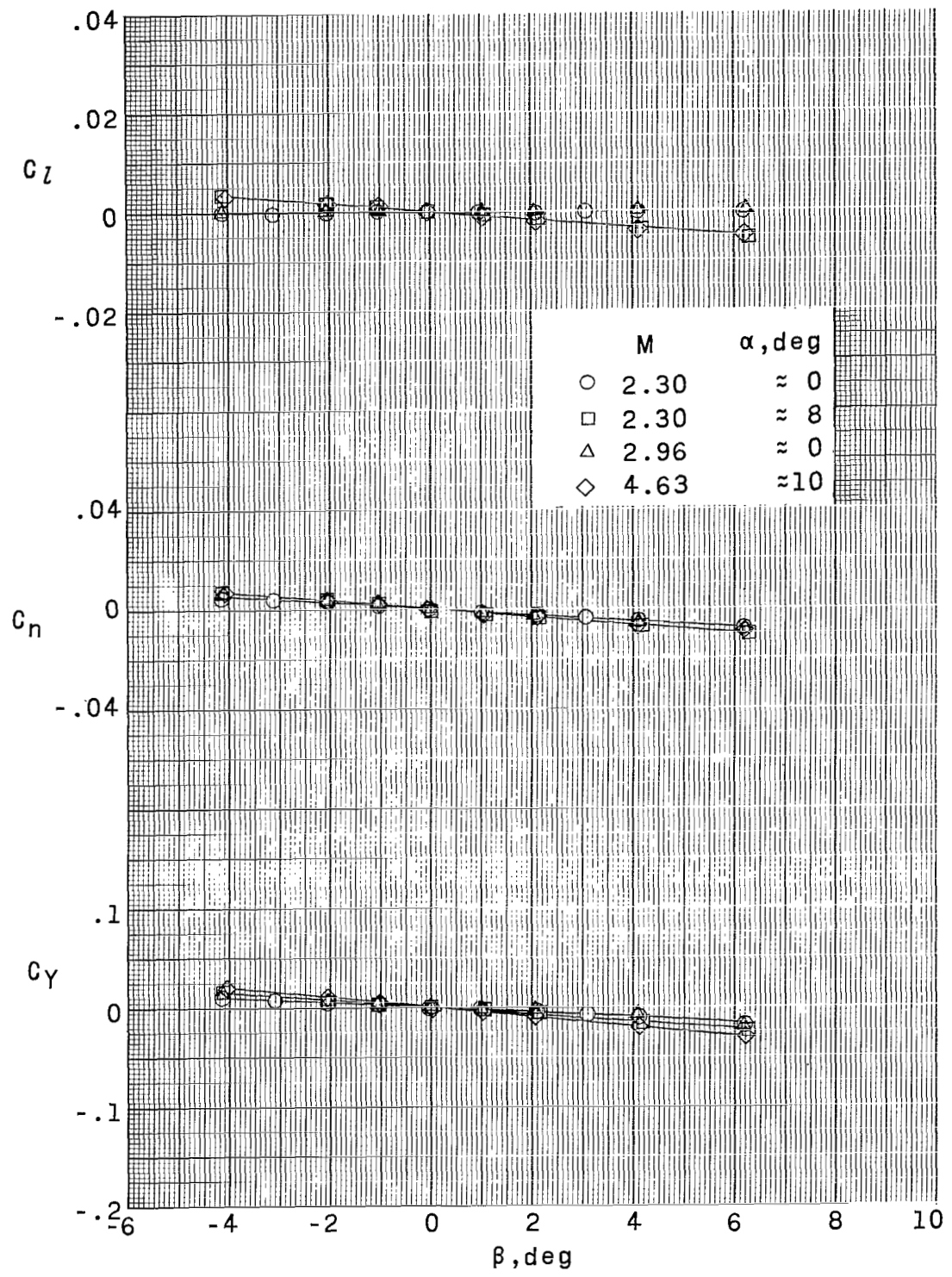


Figure 4.- Typical aerodynamic characteristics in sideslip for leading-edge configuration W<sub>6B</sub>.

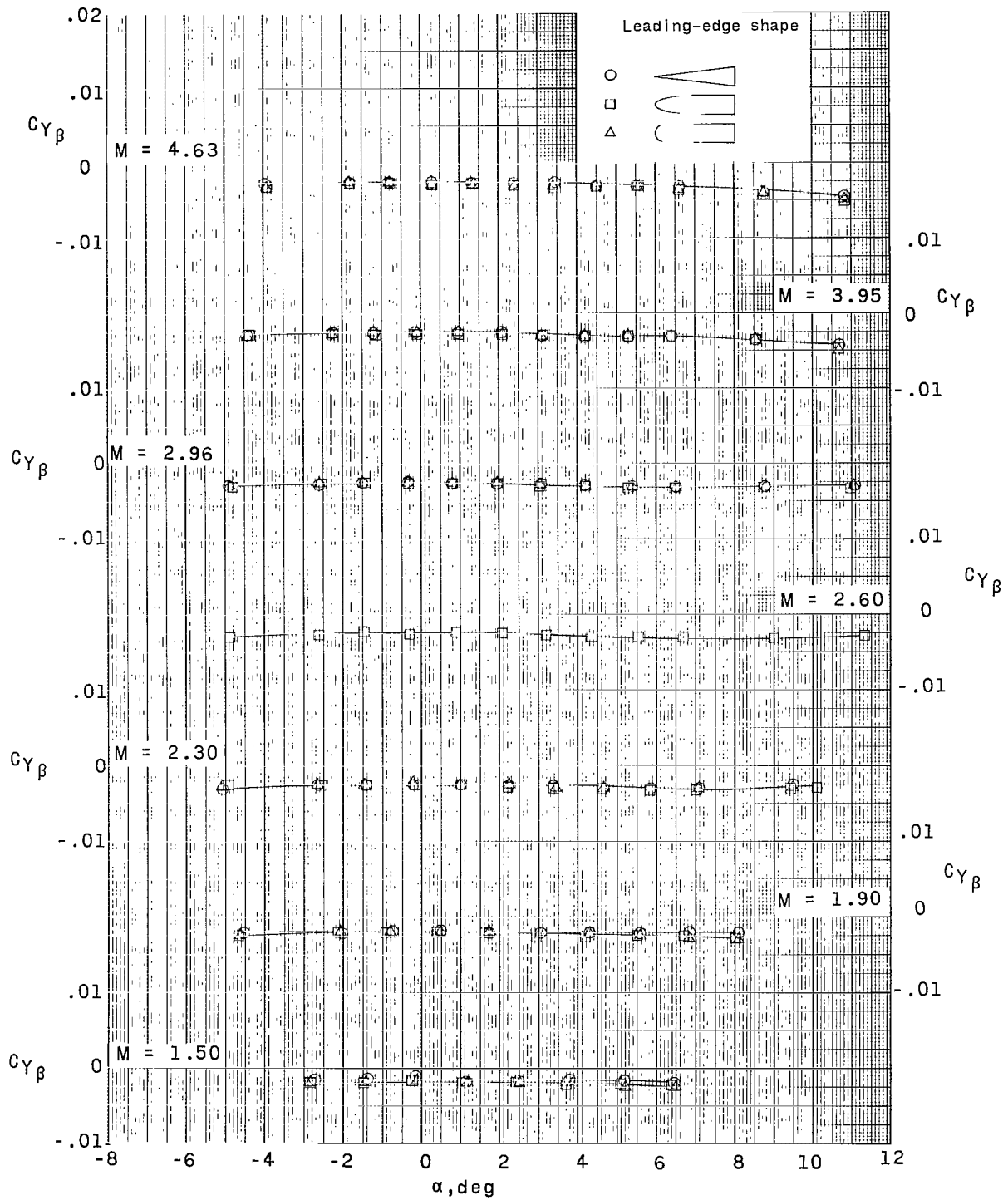


Figure 5.- Effect of leading-edge shape and Mach number on side-force parameter with angle of attack.

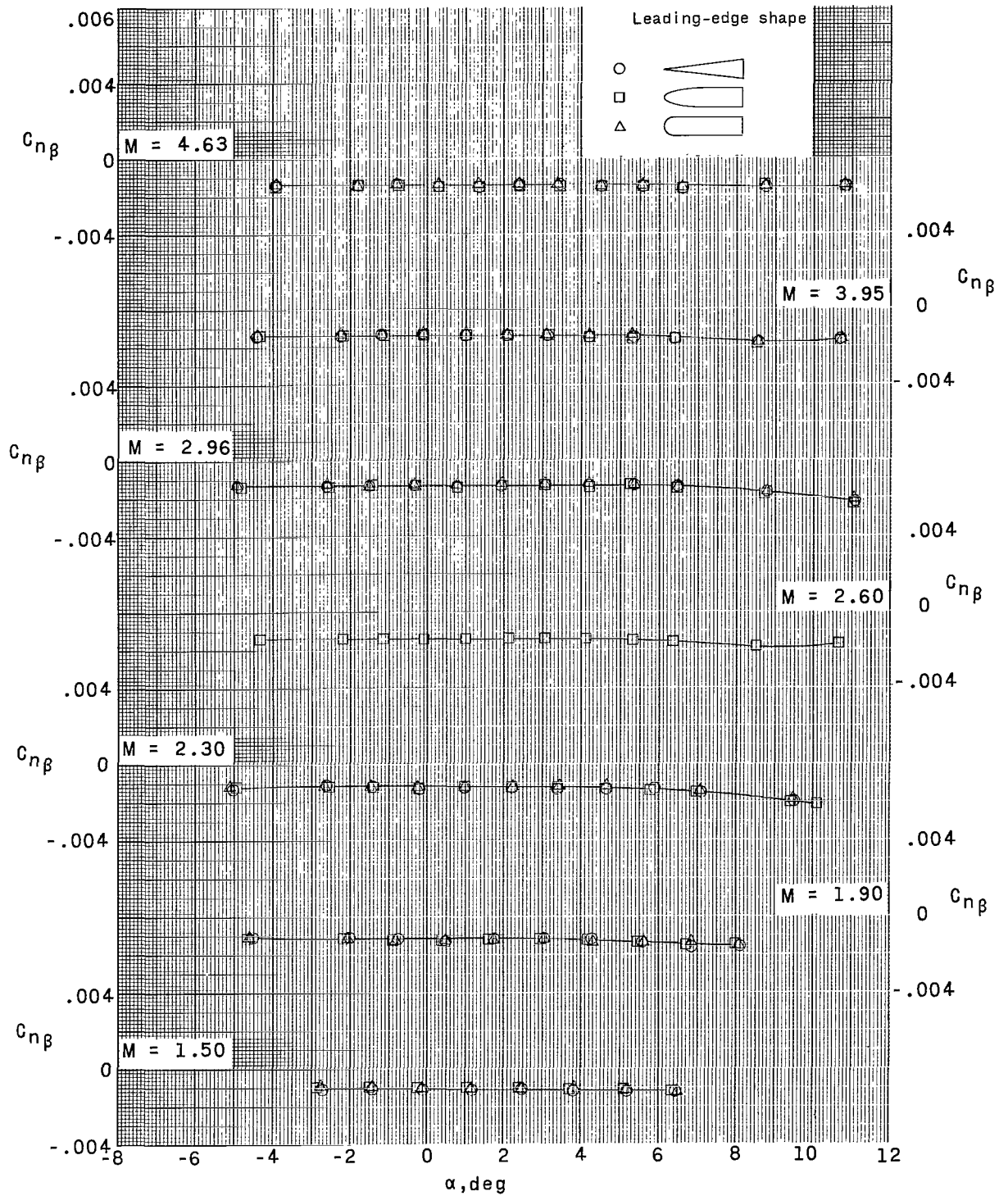


Figure 6.- Effect of leading-edge shape and Mach number on directional-stability parameter with angle of attack.

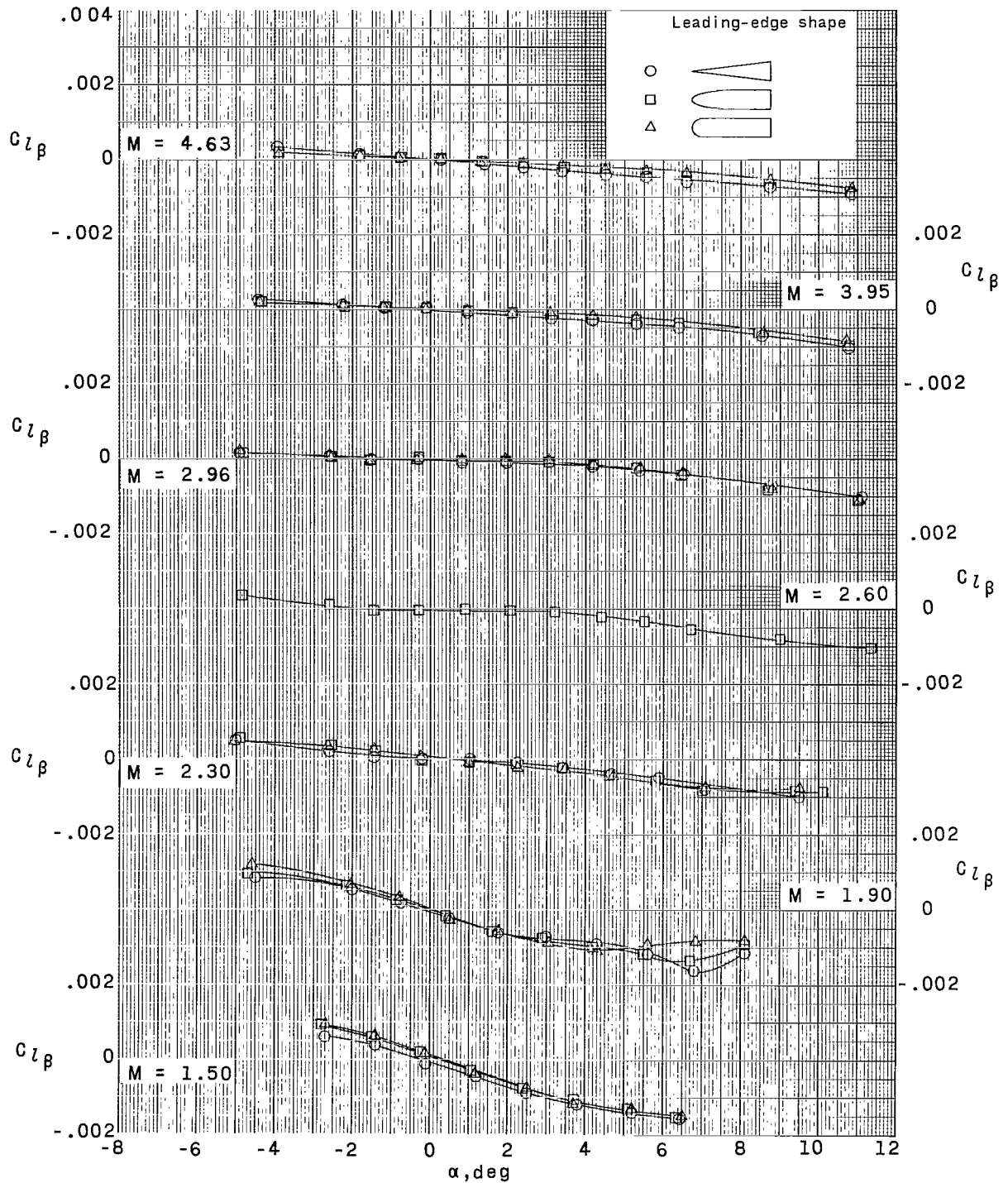


Figure 7.- Effect of leading-edge shape and Mach number on effective-dihedral parameter with angle of attack.

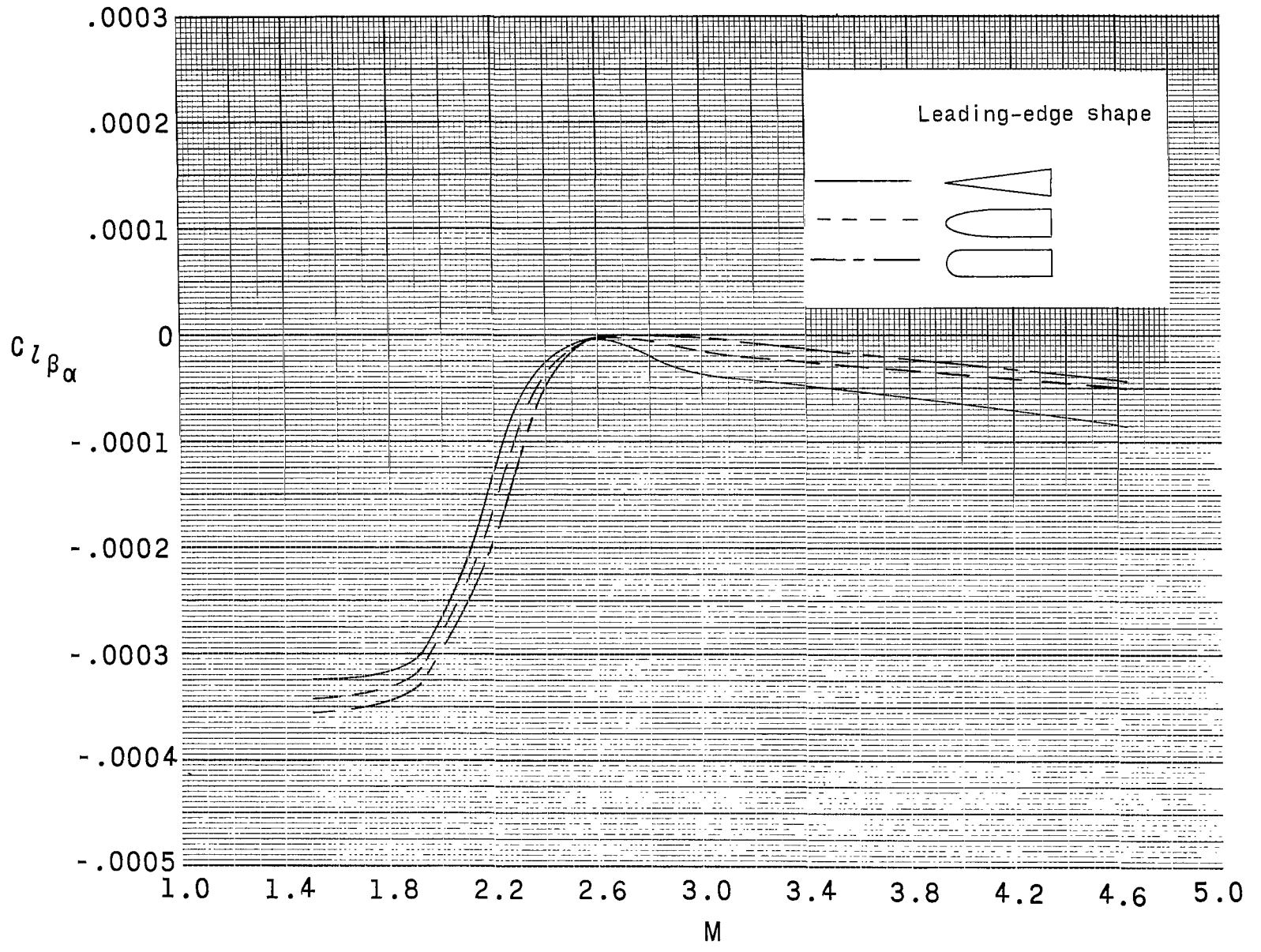


Figure 8.- Effect of leading-edge shape and Mach number on variation of slope of effective-dihedral parameter with angle of attack.